



THE UNIVERSITY *of* EDINBURGH

Edinburgh Research Explorer

## Nanocomposite-Strengthened Dissolving Microneedles for Improved Transdermal Delivery to Human Skin

**Citation for published version:**

Yan, L, Raphael, AP, Zhu, X, Wang, B, Chen, W, Tang, T, Deng, Y, Sant, HJ, Zhu, G, Choy, KW, Gale, BK, Prow, TW & Chen, X 2014, 'Nanocomposite-Strengthened Dissolving Microneedles for Improved Transdermal Delivery to Human Skin', *Advanced Healthcare Materials*, vol. 3, no. 4, pp. 555-564. <<http://onlinelibrary.wiley.com/doi/10.1002/adhm.201300312/epdf>>

**Link:**

[Link to publication record in Edinburgh Research Explorer](#)

**Document Version:**

Peer reviewed version

**Published In:**

Advanced Healthcare Materials

**General rights**

Copyright for the publications made accessible via the Edinburgh Research Explorer is retained by the author(s) and / or other copyright owners and it is a condition of accessing these publications that users recognise and abide by the legal requirements associated with these rights.

**Take down policy**

The University of Edinburgh has made every reasonable effort to ensure that Edinburgh Research Explorer content complies with UK legislation. If you believe that the public display of this file breaches copyright please contact [openaccess@ed.ac.uk](mailto:openaccess@ed.ac.uk) providing details, and we will remove access to the work immediately and investigate your claim.



1 DOI: 10.1002/adhm.((please add manuscript number))

2

3 **Nanocomposite Strengthened Dissolving Microneedles for Improved Transdermal**  
4 **Delivery to Human Skin\*\***

5

6 *By Li Yan, Anthony P Raphael, Xiaoyue Zhu, Beilei Wang, Wei Chen, Tao Tang, Yan Deng,*  
7 *Himanshu J Sant, Guangyu Zhu, Kwong Wai Choy, Bruce K Gale, Tarl W Prow, and*  
8 *Xianfeng Chen\**

9

10 [\*] Prof. Xianfeng Chen

11 Center of Super-Diamond and Advanced Films (COSDAF) and Department of Physics and  
12 Materials Science

13 City University of Hong Kong

14 Hong Kong SAR

15 E-mail: xianfeng.chen@cityu.edu.hk

16 Li Yan, Xiaoyue Zhu, Wei Chen

17 Center of Super-Diamond and Advanced Films (COSDAF) and Department of Physics and  
18 Materials Science

19 City University of Hong Kong

20 Hong Kong SAR

21 Dr. Anthony P Raphael, Dr. Tarl W Prow

22 Dermatology Research Centre

23 School of Medicine

24 The University of Queensland

25 Princess Alexandra Hospital, Brisbane,

26 Australia

27 Beilei Wang, Prof. Guangyu Zhu

28 Department of Chemistry and Biology

29 City University of Hong Kong

30 Hong Kong SAR

31 Dr. Himanshu J Sant, Prof. Bruce K Gale

32 State of Utah Center of Excellence for biomedical Microfluidics

33 Departments of Bioengineering and Mechanical Engineering

34 University of Utah

35 Salt Lake City, UT 84112,

36 USA

37 Dr. Tao Tang, Yan Deng, Prof. Richard Choy

38 Department of Obstetrics & Gynaecology

39 The Chinese University of Hong Kong

40 Hong Kong SAR

41 CUHK Shenzhen Research Institute, Shenzhen, China

42

43

44 **Keywords:** Transdermal delivery; vaccine delivery; nanocomposite; polymeric material;  
45 biomedical applications

46

47

48

**49 ABSTRACT:**

50 Delivery of drugs and biomolecules into skin has significant advantages. To achieve this,  
51 herein, we report a nanomaterial strengthened dissolving microneedle patch for transdermal  
52 delivery. The patch comprises thousands of microneedles which are composed of dissolving  
53 polymers, nanomaterials and drug/biomolecules in their interior. With the addition of  
54 nanomaterials, the mechanical property of generally weak dissolving polymers can be  
55 dramatically improved without sacrificing dissolution rate within skin. In our experiments, as  
56 a test case, we incorporated layered double hydroxides (LDH) nanoparticles into sodium  
57 carboxymethylcellulose (CMC) to form a nanocomposite. The results show that, by adding 5  
58 wt% of LDH nanoparticles into CMC, the elastic modulus of the polymer increases from  
59  $0.993\pm 0.065$  GPa to  $2.878\pm 0.123$  GPa, which is comparable to that of engineering plastics  
60 (e.g., 2.0-2.6 GPa for polycarbonate). Small and densely packed CMC-LDH microneedles  
61 penetrate human and pig skin more reliably than pure CMC ones and attractively the  
62 nanocomposite strengthened microneedles dissolve in skin and release payload within only 1  
63 minute. Finally, we tested the application of using our nanocomposite strengthened  
64 microneedle arrays for *in vivo* vaccine delivery and the results showed that significantly  
65 stronger antibody response could be induced when compared with that generated by  
66 subcutaneous injection. These data suggest that nanomaterials could be useful for fabricating  
67 densely packed and small polymer microneedles that have robust mechanical properties and  
68 rapid dissolution rate and therefore potential use in clinical applications.

**69 1. Introduction**

70 Microneedles are tiny projections of micrometer dimensions and have the capability of  
71 delivering drugs and biomolecules to skin.<sup>[1-5]</sup> This transdermal delivery platform has many  
72 advantages over conventional subcutaneous and intramuscular injection by needle and  
73 syringe. First, there is no or minimal pain, cross-infection and needle stick injuries.<sup>[6-8]</sup>

74 Second, microneedle can be designed to target specific layer of skin. Third, there is potential  
 75 for self-administration. Last but not least, it can be used when there is a significant first-pass  
 76 effect of the liver that can prematurely metabolize drugs.<sup>[9]</sup> Microneedle arrays are usually  
 77 made of silicon, metals and polymers.<sup>[10]</sup> Among them, polymer microneedle arrays are  
 78 increasingly attractive because they are expected to be less expensive to mass produce than  
 79 silicon or metal arrays and safer during application. Drugs and biomolecules can be  
 80 incorporated into the interior of microneedles themselves when using dissolving  
 81 polymers.<sup>[8,11]</sup> During application, the polymer structure rapidly dissolves in skin, thereby  
 82 releasing the drug and biomolecules, so there is no sharp waste.

83 Despite their promising features, dissolvable polymers generally have very weak  
 84 mechanical properties. The need for combination of biocompatibility, robust mechanical  
 85 properties and rapid dissolution rate severely limits the choice of polymer.  
 86 Polyvinylpyrrolidone (PVP)<sup>[1,8,11]</sup> and carboxymethylcellulose sodium salt (CMC)<sup>[7,12]</sup> are  
 87 commonly reported for making dissolving polymer microneedles. For example, PVP  
 88 microneedles were fabricated by either *in-situ* polymerization of monomers under UV  
 89 conditions (using a 100 W UV lamp) or heating at 80 °C for 24 hours.<sup>[1,8,11]</sup> These harsh  
 90 conditions may seriously limit the incorporation of drug and biomolecules that are  
 91 temperature or UV sensitive. On the other hand, CMC microneedles can be fabricated at room  
 92 temperature, but CMC has weak mechanical properties. For example, the elastic modulus of  
 93 CMC is only around 1 GPa.<sup>[12]</sup> It is expected that the bioresorbable polymer microneedle size  
 94 needs to be relatively large to reliably pierce human skin.<sup>[12]</sup> This would apparently constrain  
 95 the density of microneedles on an array. However, recent study shows that small (base  
 96 diameter or width < 40 μm) and densely packed microneedles (over 10,000 microneedles per  
 97 cm<sup>2</sup>) may lead to significantly enhanced vaccine efficacy when compared to large and  
 98 sparsely packed ones.<sup>[13,14]</sup> In addition, small microneedles can be easily dried during

99 fabrication and dissolve rapidly in skin during application. Therefore, improving the  
 100 mechanical properties of dissolving polymer microneedles could be beneficial in terms of  
 101 drug efficacy and design flexibility as well as ease in fabrication and rapid dissolution in the  
 102 skin.

103 To achieve this, we hypothesize that the use of reinforcing nanofillers will result in an  
 104 advanced biomedical material that can make enhanced dissolving polymer microneedles that  
 105 are mechanically more robust, while retaining the capacity to rapidly dissolve. Layered  
 106 double hydroxide (LDH) nanoparticles have been commonly used to reinforce a variety of  
 107 polymers.<sup>[15]</sup> For example, by adding only 1 wt% of LDH nanoparticles into nylon 6, the  
 108 elastic modulus of the composite increases 100% in comparison with that of pure nylon 6  
 109 polymer.<sup>[16]</sup> Therefore, in this paper, we have examined the potential for LDH nanoparticles  
 110 to enhance the mechanical strength of CMC cast in microneedle arrays for potential drug and  
 111 biomolecule delivery. We are the first to report the use of nanomaterials to improve the  
 112 mechanical characteristics of dissolving microneedle arrays for transdermal delivery.

## 113 **2. Results**

### 114 **2.1. Characterization of Mg<sub>2</sub>Al-CI-LDH Nanoparticles**

115 We firstly prepared Mg<sub>2</sub>Al-CI-LDH nanoparticles with a mean size of 80 nm and zeta  
 116 potential of +40 mV in aqueous and buffer-free solution (**Figure 1a-c**). The as-prepared  
 117 aqueous suspension contained well suspended LDH nanoparticle without aggregation (Figure  
 118 1a-b). XRD pattern shows the typical feature of Mg<sub>2</sub>Al-CI-LDH nanoparticles (Figure 1d).  
 119 Diffraction peaks shown in the XRD pattern of pristine LDH nanoparticles correspond to the  
 120 (003), (006) and (009) plane reflections of LDH.

### 121 **2.2. Mechanical Properties of CMC and CMC-LDH Nanocomposite**

122 We incorporated varying amounts of LDH into 2 wt% CMC aqueous solution to test the  
 123 strengthening effect of LDH nanoparticles on the mechanical properties of CMC. After the  
 124 samples were dried, nanoindentation was used to measure their elastic modulus and hardness.  
 125 **Figure 2a** shows typical load–displacement curves of CMC polymer with different  
 126 concentrations of LDH nanoparticles. The nanoindentation cycle consists of three periods:  
 127 loading-holding-unloading. Loading forces were increased at constant velocity and the  
 128 nanoindenter tip sank into materials during the loading period, which contributed to both  
 129 elastic and plastic deformation. Strong materials require a high force to achieve the same  
 130 penetration depth during the loading period.<sup>[16]</sup> As we can observe from Figure 2a, much  
 131 greater load is required for penetration of the same depth as LDH nanoparticle concentration  
 132 increases from 0 wt% to 2, 5 and 10 wt% (relative to the mass of CMC in the samples).  
 133 Apparently, adding LDH nanoparticles into CMC can significantly enhance its resistance to  
 134 indentation and make CMC-LDH composite much stronger than pure CMC. Figure 2b and  
 135 Figure 2c show the elastic modulus and hardness of polymers, respectively, calculated from  
 136 unloading. The elastic modulus of pure CMC is  $0.993 \pm 0.065$  GPa. The elastic modulus of 2  
 137 wt% of LDH loaded CMC increased to  $1.489 \pm 0.036$  GPa. With LDH concentration increased  
 138 to 5 wt%, the elastic modulus reaches  $2.878 \pm 0.123$  GPa. The elastic modulus increased to  
 139 290% of that of pure CMC polymer when 5 wt% of LDH nanoparticles were added to CMC  
 140 ( $p < 0.001$ ). When the LDH concentration was increased to 10 wt%, the elastic modulus of  
 141 the nanocomposite started to decrease. It should be noted that the hardness of pure CMC  
 142 polymer is  $0.067 \pm 0.001$  GPa. The addition of LDH nanoparticles to CMC increased the  
 143 hardness of the composite material to  $0.080 \pm 0.001$  GPa,  $0.111 \pm 0.004$  GPa and  $0.118 \pm 0.001$   
 144 GPa for CMC composites with 2 wt%, 5 wt% and 10 wt% of LDH nanoparticles,  
 145 respectively.

146 Based on these results we chose the CMC composite with 5 wt% LDH nanoparticles as  
 147 the starting material for preparing microneedle arrays. Since centrifugation ( $3000 \times g$  for 10  
 148 minutes) was used to force the viscous polymer solution to fill in the tiny cavity of a  
 149 microneedle PDMS mold, the concentration of CMC aqueous solution was increased to 5  
 150 wt% to avoid unequal LDH nanoparticle distribution within the centrifuged microneedles.  
 151 When 5 wt% LDH (relative to the mass of CMC) was added to the 5wt% CMC solution  
 152 followed by centrifugation at  $4000 \times g$  for 10 minutes, negligible amount of LDH  
 153 nanoparticles was sedimented by simply observing the mixture solution. The bottom layer of  
 154 the solution was discarded and supernatant was used for nanoindentation measurements. The  
 155 results show that the elastic modulus of 5 wt% CMC/5 wt% LDH was  $2.486 \pm 0.186$  GPa. The  
 156 value is slightly lower than the highest elastic modulus of the sample dried from the solution  
 157 of 2 wt% CMC incorporating with 5 wt% LDH, but it is still much better than that of pure  
 158 CMC ( $p < 0.001$ ). The suspension of 5 wt% CMC/5 wt% LDH was then used for fabricating  
 159 microneedles.

### 160 **2.3 Characterization of CMC-LDH Nanocomposite Microneedle Patches**

161 The validation of the hypothesis that incorporation of LDH nanoparticles into CMC  
 162 could significantly increase the mechanical properties of the polymer supported the use of this  
 163 nanofiller-improved polymer to fabricate and test microneedle arrays. **Figure 3a** and Figure  
 164 3b are representative SEM images of silicon microneedle male molds used to prepare PDMS  
 165 female molds for polymer microneedle fabrication. The height and density of silicon  
 166 microneedles are  $218 \mu\text{m}$  and  $11,900$  projections  $\text{cm}^{-2}$ , respectively. Figure 3c and Figure 3d  
 167 show typical SEM images of our dissolving polymer microneedles. The polymer  
 168 microneedles had uniform morphology and geometry. The microneedles were pyramidal in  
 169 shape and the tip radius is below  $500 \text{ nm}$ . The length of these fabricated polymer projections  
 170 is  $165 \pm 3 \mu\text{m}$  ( $n=20$  projections). This indicates a  $24 \pm 1\%$  reduction in length in comparison

171 with that of the microneedles of the male mold. This decrease is mainly due to the contraction  
172 and solidification of CMC based composite materials during drying.

173 **2.4. Confocal Microscopy Study of the Penetration and Payload Delivery of**  
174 **Nanocomposite Microneedle Patches in Human and Pig Skin**

175 Once nanocomposite microneedle patches were successfully made, the next key  
176 question was whether these microneedles can reliably penetrate stratum corneum and delivery  
177 payload to skin? To perform this study, FITC-Dextran was simply mixed with CMC-LDH  
178 nanoparticle solution as a viewable drug and biomolecule surrogate and then cast onto the tips  
179 of microneedles and then we tested nanofiller composite microneedle penetration in excised  
180 pig and human skin. To determine whether the microneedles can uniformly penetrate skin,  
181 reflectance confocal microscopy (RCM) was used to image both the treated pig skin and  
182 human skin (representative images shown in **Figure 4a-d**). Nanocomposite microneedles  
183 applied to *pig* skin resulted in successful breaching of the stratum corneum and uniform  
184 penetration within the skin across the array (Figure 4a). The penetration depth analyzed from  
185 the RCM images was  $71 \pm 7 \mu\text{m}$  ( $n = 40$  projections). These results differed from what was  
186 observed for the CMC only microneedles where the penetration was not uniform (Figure 4b).  
187 The center area shows penetration but no penetration holes are able to be clearly observed in  
188 the rest area. The depth of the penetration in the center area was found to be  $46 \pm 12 \mu\text{m}$  ( $n =$   
189  $40$  projections,  $p < 0.001$  between CMC and CMC-LDH microneedles penetration in pig  
190 skin). The nanocomposite microneedles also resulted in successful breaching and penetration  
191 into *human* skin (Figure 4c) with a depth of  $64 \pm 9 \mu\text{m}$  ( $n = 40$  projections). The CMC only  
192 microneedles resulted in indents on the skin surface with minimal penetration of  $39 \pm 8 \mu\text{m}$  ( $n$   
193  $= 40$  projections,  $p < 0.001$  between CMC and CMC-LDH microneedle penetration in human  
194 skin) (Figure 4d). Besides achieving apparent deeper penetration depth in both pig and human  
195 skin, CMC-LDH nanocomposite microneedles can be more reliable on successful application



196 while CMC microneedles result in inconsistent penetration across the array, due to the  
197 microneedles bending on skin surface sometimes.

198 The RCM samples were then imaged using laser scanning confocal microscopy  
199 (LSCM) to determine payload dissolution and diffusion within the skin (representative images  
200 shown in **Figure 5a-h**). For pure CMC microneedle applied skin samples, the images were  
201 selected from the area where penetration of microneedles into skin was achieved. The  
202 delivery sites are clearly observed from the top view of the skin samples (Figure 5a, 5c, 5e  
203 and 5g), which further confirms the polymer microneedles are able to pierce stratum corneum.  
204 For some delivery sites, it is obvious to see the holes created by the microneedle penetration.  
205 The corresponding 3-D images (Figure 5b, 5d, 5f and 5h) clearly show that the FITC payload  
206 was delivered vertically to certain depths beneath the skin surface. In a number of delivery  
207 sites, it is even possible to see that the delivery payload started to diffuse a lot within the skin  
208 after only 5 minutes. Collectively, Figure 5 demonstrates that the microneedles were capable  
209 of piercing stratum corneum followed by dissolving in the skin and delivering the FITC  
210 payload to the thin layer beneath the skin surface.

211 Now we have confirmed that the CMC-LDH nanocomposite microneedles can reliably  
212 penetrate skin and deliver the payload into skin. Compared with CMC microneedles, the  
213 nanomaterial strengthened microneedles result in more consistent penetration within the skin  
214 cross the whole patch area. Another key question is whether these mechanically strengthened  
215 microneedles can still rapidly dissolve in skin? To investigate this, we observed the  
216 microneedles before application in skin and at 1, 2 and 5 minutes after skin penetration. The  
217 results are shown in **Figure 6**. The figure shows the merged fluorescence and reflectance  
218 confocal microscopy images of microneedles before and after being applied to skin. Before  
219 application, the fluorescent payload can be clearly seen in green throughout the shaft of the  
220 microneedles (Figure 6a). No fluorescence signal could be detected at the base of the array,

221 which has the added benefit of reducing cost through conserving drug molecules to the  
 222 microneedles only and therefore reducing drug wastage during delivery. Because of this, in  
 223 our experiments, minimal fluorescence was seen on the surface between the microneedles due  
 224 to the payload being cast within the projections instead of ‘wasted’ in the backing layer of the  
 225 microneedles. After skin application, it can be seen that almost all of the microneedles are  
 226 dissolved in the skin after only 1 minute.

227 **2.5. In vivo Delivery of Antigen to Skin and Successful Immunization of Mice**

228 Having confirmed that our nanocomposite microneedles can robustly penetrate, quickly  
 229 deliver payload to human and pig skin and target specific skin layers, next we test the  
 230 application of the nanocomposite microneedle arrays for vaccine delivery. We fabricated  
 231 CMC and CMC-LDH microneedle arrays with 10 and 1.65  $\mu\text{g}$  of ovalbumin (OVA) protein,  
 232 respectively. Pure CMC polymer microneedle arrays were used as a control in the experiment.  
 233 Mice were anesthetized and a single microneedle patch was applied to each ear, therefore 2  
 234 microneedle patches were used for each mouse. As a positive control, we subcutaneously  
 235 injected 20 $\mu\text{g}$  of OVA protein to mice. The induced antibody titers of mice are shown in  
 236 **Figure 7**. From the figure, the following can be observed. At 14 days after primary  
 237 immunization, subcutaneous (SC) injection of 20  $\mu\text{g}$  of OVA protein induced negligible  
 238 immune response compared with that of unimmunized mice. In great contrast, both CMC and  
 239 CMC-LDH microneedle vaccination led to great immune response indicated by the high  
 240 antibody titer shown in Figure 7a. The antibody titers between the two microneedle  
 241 immunized groups do not show statistical difference ( $p > 0.1$ ). If we compare the standard  
 242 error of the mean of the two microneedle groups, it is easy to find that the antibody titers  
 243 generated by CMC-LDH microneedle patch vaccination are more consistent than those  
 244 induced by CMC microneedle immunization.

245           The mice were then boosted at 17 days after primary immunization and sera were  
 246 collected at 21 days after the boost (38 days after primary vaccination). From Figure 7b, it can  
 247 be seen that, after boost, SC injection of 20  $\mu\text{g}$  of OVA protein led to reasonably high  
 248 antibody titers, although still much lower than those induced by microneedle vaccination ( $p <$   
 249 0.001). The other finding is that, after boost, CMC-LDH microneedle arrays containing 3.3  $\mu\text{g}$   
 250 of OVA protein led to stronger immune response than that induced by pure CMC microneedle  
 251 patches with 20  $\mu\text{g}$  of OVA protein ( $p < 0.001$ ).

### 252   **3. Discussion**

253           In this paper, we hypothesized that the LDH nanoparticles could enhance the  
 254 mechanical properties of CMC microneedles and thereby improve transdermal delivery. We  
 255 chose CMC because it had often been used as a material in dissolving microneedles<sup>[7,12]</sup> in the  
 256 literature, but the elastic modulus of CMC is only 1 GPa<sup>[12]</sup>, which potentially limits the  
 257 successful application of CMC microneedles in transdermal drug and biomolecule delivery  
 258 for humans, particularly when one needs to fabricate densely packed microneedles for certain  
 259 needs. LDH nanoparticles were selected to increase the mechanical strength of CMC because  
 260 of their high biocompatibility, high aspect ratio (lateral size over thickness), low cost and  
 261 previous use in enhancing mechanical strength in polymers.<sup>[15-17]</sup> Furthermore, CMC is  
 262 negatively charged in solution and may well be incorporated into the internal layers of LDH  
 263 nanoparticles and help disperse LDH nanoparticles uniformly. Consistent dispersion is a  
 264 crucial challenge when formulating nanofillers to mechanically strengthen polymers as better  
 265 dispersion of nanomaterials/fillers leads to enhanced mechanical properties.<sup>[15]</sup> The  
 266 mechanical strength of CMC was greatly enhanced by adding LDH nanoparticles. The elastic  
 267 modulus of our CMC-LDH composite microneedles is comparable to that of engineering  
 268 plastics, e.g. 2–4 GPa for nylon and 2.0-2.6 GPa for polycarbonate. This improvement has the  
 269 capacity to increase the flexibility of drug and molecule formulations that can be incorporated

270 into dissolving microneedle arrays. It is expected that the addition of drug and molecules,  
 271 composed primarily of proteins and salts, will worsen the mechanical properties of the  
 272 structural polymer in a concentration dependent manner. The addition of reinforcing  
 273 nanofillers could help to curb that effect such that the final microneedle array remains useful  
 274 for animal and human applications.

275 Our fabrication process was operated at room temperature (23 °C). Lowering the  
 276 temperature to optimize the stability of the drugs and molecules could be explored using this  
 277 casting technique. The entire fabrication process required no heating, UV illumination or any  
 278 other harsh conditions or treatments and therefore our technique is suitable for incorporating  
 279 delicate drugs and biomolecules into microneedles for subsequent transdermal delivery. The  
 280 enhanced mechanical properties of the CMC-LDH composite microneedles successfully  
 281 pierced pig and human skin to deliver a FITC-labeled dextran payload. Importantly, the  
 282 nanoparticle strengthened polymer microneedles retained the capacity to dissolve quickly,  
 283 within only 1 minute. Quick dissolution within skin is crucial for a short administration time.  
 284 For comparison, in a previous report, methacrylic acid (MAA) was copolymerized with vinyl  
 285 pyrrolidone (VP) to form poly(vinylpyrrolidone-co-methacrylic acid) (PVP-MAA) to improve  
 286 the mechanical strength of the fabricated microneedles. However, with the addition of MAA,  
 287 the dissolution rate of the microneedles greatly slowed. For example, PVP-MAA  
 288 microneedles (25% MAA) need 2 hours to dissolve within porcine skin while at the same size  
 289 pure PVP microneedles dissolve within 15 minutes.<sup>[8]</sup>

290 Skin contains abundant of immune cells and the density of these cells is much high than  
 291 that in subcutaneous tissue and muscle to which vaccines are usually delivered by needle and  
 292 syringe injection. Therefore, if we can deliver vaccines to the skin layers, their efficacy should  
 293 be greatly enhanced. Although it is possible to use conventional needle and syringe to achieve  
 294 intradermal injection for delivering vaccine to the skin, it is technically challenge to perform

295 because the skin is very thin. To achieve reliable skin delivery, many approaches such as  
 296 liquid jet injection, biolistic microparticle injection, thermal or laser assisted delivery and  
 297 microneedles have been developed. <sup>[18]</sup> When these approaches were tested for vaccine  
 298 delivery to skin and compared with conventional intramuscular (IM) or SC injection, it was  
 299 found that the vaccine efficacy was dramatically improved. <sup>[19-22]</sup> To test whether our  
 300 nanocomposite strengthened microneedle arrays can pierce skin and deliver payload to the  
 301 targeted skin layers, we investigated the penetration and payload delivery by RCM and  
 302 LSCM. The results confirmed that the composite microneedles successfully penetrated  
 303 stratum corneum and delivered the FITC-labeled dextran payload up to around  $64\pm 9\ \mu\text{m}$   
 304 below the human skin surface. The human epidermis layer contains high density of APCs and  
 305 its thickness, using human forearm dorsal epidermis as an example, is  $61.3\pm 11.0\ \mu\text{m}$ .<sup>[23]</sup> This  
 306 means that most of the payload was delivered within the target layer.

307         Once demonstrating that the nanocomposite strengthened microneedle arrays could  
 308 deliver payload to skin, next key question will be whether they can induce robust immune  
 309 response. To investigate this, we loaded OVA protein in the microneedle arrays and  
 310 performed immunization trial in mouse model. The results suggested that dissolvable pure  
 311 CMC microneedle patches could induce much stronger immune response when compared  
 312 with conventional efficient SC injection (generally more efficient than the commonly used  
 313 intramuscular injection). Attractively, it was confirmed that the nanocomposite strengthened  
 314 microneedle arrays worked even better than the pure dissolvable ones. This is in line with the  
 315 findings from the penetration experiments. Because nanocomposite strengthened microneedle  
 316 arrays could penetrate skin better and worked more reliably, it was apparent that the  
 317 strengthened arrays should deliver more vaccine dose into skin. In other words,  
 318 nanocomposite strengthened microneedle arrays were capable of increasing vaccine delivery  
 319 efficiency.

320 Moreover, LDH nanoparticles have been widely used for efficient delivery of a range of  
 321 drugs such as anticancer drug methotrexate (MTX),<sup>[24,25]</sup> low molecular weight heparin  
 322 (LMWH),<sup>[26]</sup> siRNA<sup>[27-29]</sup> and plasmid DNA.<sup>[30,31]</sup> The biocompatibility and safety profiles  
 323 obtained these studies will certainly help the potential use of LDH nanoparticles in our  
 324 nanocomposite microneedle arrays in future clinical applications. In the meantime, it also  
 325 opens the opportunity of incorporating vaccine into LDH nanoparticles for transdermal  
 326 nanovaccine delivery. This will be very suitable for DNA and siRNA delivery because these  
 327 molecules need to enter cells to be functional and their existence in nanovaccine form will  
 328 greatly increase their intracellular delivery. In this case, LDH nanoparticles will play  
 329 multifunctional roles including mechanical strengthening and nanovaccine carrier.

#### 330 **4. Conclusion**

331 In this study, we demonstrated that LDH nanoparticles can reinforce dissolving polymer  
 332 microneedles. By adding 5 wt% of LDH into CMC, the elastic modulus increases from  
 333 0.993±0.065 GPa to a maximum of 2.878±0.123 GPa ( $p < 0.001$ ). Additionally, we  
 334 successfully manufactured LDH nanoparticle-reinforced, dissolving polymer microneedles  
 335 with uniform shape and size. The polymer microneedles have an extremely sharp tip with an  
 336 average radius below 500 nm. The fabrication process was conducted at room temperature  
 337 without the need for any harsh conditions that may degrade drugs and biomolecules. Confocal  
 338 microscopy results confirmed that the nanofiller strengthened the dissolving microneedles by  
 339 improving their mechanical properties to allow the microneedles to reliably pierce into pig  
 340 and human skin, while pure CMC polymer microneedle were more likely to bend on the  
 341 surface of skin. The composite microneedles retained the capacity to dissolve rapidly in skin  
 342 within only 1 minute and released the incorporated payload. The payload distribution was  
 343 highly localized within the skin. Finally, we tested the application of using our nanocomposite  
 344 strengthened microneedle arrays for vaccine delivery and the results showed that significantly

345 stronger antibody response could be induced when compared with subcutaneous injection.  
 346 Overall, this represents an important step toward dissolving microneedles that have robust  
 347 mechanical properties with potential use in clinical applications.

#### 348 **4. Experimental Section**

349 *Preparation of Mg<sub>2</sub>Al-LDH Nanoparticles:* Mg<sub>2</sub>Al-LDH nanoparticles were prepared  
 350 according to the method described by Xu et al.<sup>[32,33]</sup> Briefly, 40 ml of 0.15 M NaOH  
 351 (International Laboratory, USA) solution was mixed with 10 ml of solution containing 2.0  
 352 mmol of MgCl<sub>2</sub> (International Laboratory, USA) and 1.0 mmol of AlCl<sub>3</sub> (International  
 353 Laboratory, USA) under vigorous stirring. The container was sealed and the solution was  
 354 under stirring for 10 minutes. Next, the solution was centrifuged and washed once with water.  
 355 The obtained slurry was dispersed in 40 ml of water and hydrothermally treated at 80 °C for 4  
 356 hours in an airtight container. The concentration of LDH is about 0.4 wt%. The mass of LDH  
 357 was determined by weighing the LDH mass collected from suspension.

358 *Fabrication of CMC-LDH Nanocomposites:* LDH solutions with different concentrations  
 359 were mixed with CMC (Mw 90,000, Sigma-Aldrich, USA) to make composite solution.  
 360 Briefly, 10 ml of LDH solutions with different concentrations were mixed with 200 mg of  
 361 CMC to prepare composite solution followed by placing in fume hood and drying to obtain  
 362 polymer nanocomposite. The prepared nanocomposites contained 2 wt%, 5 wt% and 10 wt%  
 363 LDH nanoparticles. The weight percentage is the mass ratio of LDH nanoparticles to CMC.  
 364 During microneedle fabrication, CMC-LDH solution was centrifuged onto the mold at a  
 365 speed of 3000 × g for 10 minutes. To mimic this process, for another batch of samples, 10 ml  
 366 of solution containing 25mg LDH nanoparticles was mixed with 500 mg of CMC and the  
 367 mixture was sonicated for 30 minutes. After that, the solution was centrifuged for 10 min at  
 368 4000 × g. The amount of the nanoparticles which were centrifuged to the bottom of solution

369 was trivial. The upper layer of solution was collected and sonicated for 30 minutes for being  
 370 used to make nanoindentation samples and microneedle arrays.

371 *Fabrication of Dissolving Polymer Microneedle Patches:* Silicon microneedle arrays  
 372 were used as male mold. The arrays were fabricated according to methods described in  
 373 literature.<sup>[34]</sup> Briefly, a silicon wafer was diced by a diamond blade to create silicon  
 374 microcolumns of required dimension and spacing. A two-step isotropic etching using a  
 375 mixture of nitric acid and hydrofluoric acid was used to fabricate sharp microneedles. This  
 376 silicon microneedle array male mold was washed with ethanol for 3 times and dried in air and  
 377 then PDMS was slowly poured over the surface of silicon microneedle array. The silicon  
 378 microneedle array male mold immersed in PDMS was placed in a fume hood for curing for 24  
 379 hours. After curing, the silicon microneedle array male mold was peeled off and the PDMS  
 380 female mold was washed with water and ethanol for 3 times before casting. **Figure 8** shows  
 381 the steps to manufacture a dissolving polymer microneedle patch. Figure 8-1 shows the  
 382 PDMS mold. To make microneedle patches, firstly, 30  $\mu\text{l}$  of LDH-CMC composite solution  
 383 was added to the surface of mold (Figure 8-2). Then the mold was sealed (Figure 8-3) and  
 384 centrifuged at  $3000 \times g$  for 10 minutes. After centrifugation, the solution remaining on the  
 385 surface of the mold was collected by pipette and the mold was placed in a fume hood to dry  
 386 for 30 minutes. During the drying period, a solid microneedle tip was fabricated (Figure 8-5).  
 387 Subsequently, 40  $\mu\text{l}$  of LDH-CMC composite solution was added to the surface (Figure 8-6)  
 388 and the mold was sealed (Figure 8-7) and centrifuged for 10 minutes. Finally, 200  $\mu\text{l}$  of LDH-  
 389 CMC composite solution was added to the surface of centrifuged mold and placed in a fume  
 390 hood for drying. After 8 hours, the mold was placed in a sealed desiccator. When the  
 391 microneedle patch was dried completely, it was removed from the mold (Figure 8-9) and  
 392 stored in a dessicator until use.



393            *Characterization:* Nanoindentation was carried by a MTS Nano Indenter XP® (MTS  
394 Cooperation, Nano Instrument Innovation Center, NT) with three-sided pyramid (Berkovich)  
395 diamond indenter. The indenter was pressed into materials with constant strain rate (0.05 1/s)  
396 from the sample surface into 2000 nm deep. The fabricated polymer microneedle patch was  
397 observed by scanning electron microscope (JEOL JSM-820 and FEG-SEM JEOL JSM-6335  
398 F). The samples were tilted 45° for SEM.

399            *Microneedle Application to Excised Skin:* Excised pig ears were obtained from the local  
400 abattoir (Highchester Pty Ltd, Gleneagle, Australia). The ventral side of the ear was lightly  
401 shaved followed by thoroughly rinsing. The ventral skin (epidermis and dermis) was then  
402 separated from the ear (cartilage) using tweezers and scalpel. Excised human skin was  
403 obtained from abdominal plastic surgery patients. On arrival the adipose tissue was removed  
404 using a scalpel and the skin was rinsed. All patients signed an informed consent approved by  
405 the Princess Alexandra Hospital Research Committee approval no. 097/090. Skin (both pig  
406 and human) was stored at -20 °C prior to use. For microneedle application, the skin (pig or  
407 human) was thawed, rinsed, dried then pinned down taut on a covered corkboard. The tissue  
408 was stored on saline moistened gauze throughout the experiment when not in use. A  
409 microneedle array was then applied using a spring applicator for 1, 2 or 5 minutes (n = 3 per  
410 skin type). After microneedle application, the treatment area was excised with an 8 mm  
411 biopsy and the tissue fixed in 1 mL 4% formaldehyde in methanol for 1 hour. Following  
412 fixing, the tissue was removed and washed 3 times for 10 minutes in 1 mL 0.1M phosphate  
413 buffered saline. The samples were then stored at 4 °C until imaging.

414            *Confocal Microscopy Observation of Skin after Patch Application:* Reflectance confocal  
415 microscopy was done using a Vivascope® 1500 Multilaser (Lucid Inc., Rochester, NY,  
416 U.S.A). The protocol was adapted from a previously published procedure.<sup>[35]</sup> Briefly, a laser

417 diode was used to excite the tissue at 830 nm. ImageJ (NIH, U.S.A) was used to analyse the  
 418 images. Laser scanning confocal microscopy was done using a Zeiss LSM 510 Meta (Carl  
 419 Zeiss Inc., Germany). Prior to imaging the tissue was stained with Hoechst 33342, a nuclei  
 420 stain. A stock solution of 10 mg/mL Hoechst 33342 in dimethyl sulfoxide was prepared. A  
 421 working solution was made by a 1:1000 dilution in 0.1 M phosphate buffered saline. The  
 422 tissue was incubated with the stain for 1 hour at room temperature followed by three washing  
 423 steps for 10 minutes in 0.1 M phosphate buffered saline. The wavelengths used to excite the  
 424 FITC-dextran and Hoechst 33342 was 488 nm and 405 nm, respectively.

425 *Vaccination of OVA protein vaccine:* Three groups of C57BL/6 female mice were  
 426 vaccinated with OVA protein either by SC injection using needle and syringe (5 mice in the  
 427 group), or microneedle array application (4 mice per group). Another group of four untreated  
 428 mice were used as negative control. For SC injection, saline solution with 20 µg OVA protein  
 429 was injected to each mouse. For microneedle array vaccination, one patch was applied to one  
 430 ear of a mouse (total 2 patches for each mouse). The patches were applied to mice skin by a  
 431 spring applicator and kept in place for 2 minutes. At 14 days after primary immunization, sera  
 432 were collected. A boost vaccination was given at 17 days post primary vaccination and sera  
 433 were collected at 21 days after the boost.

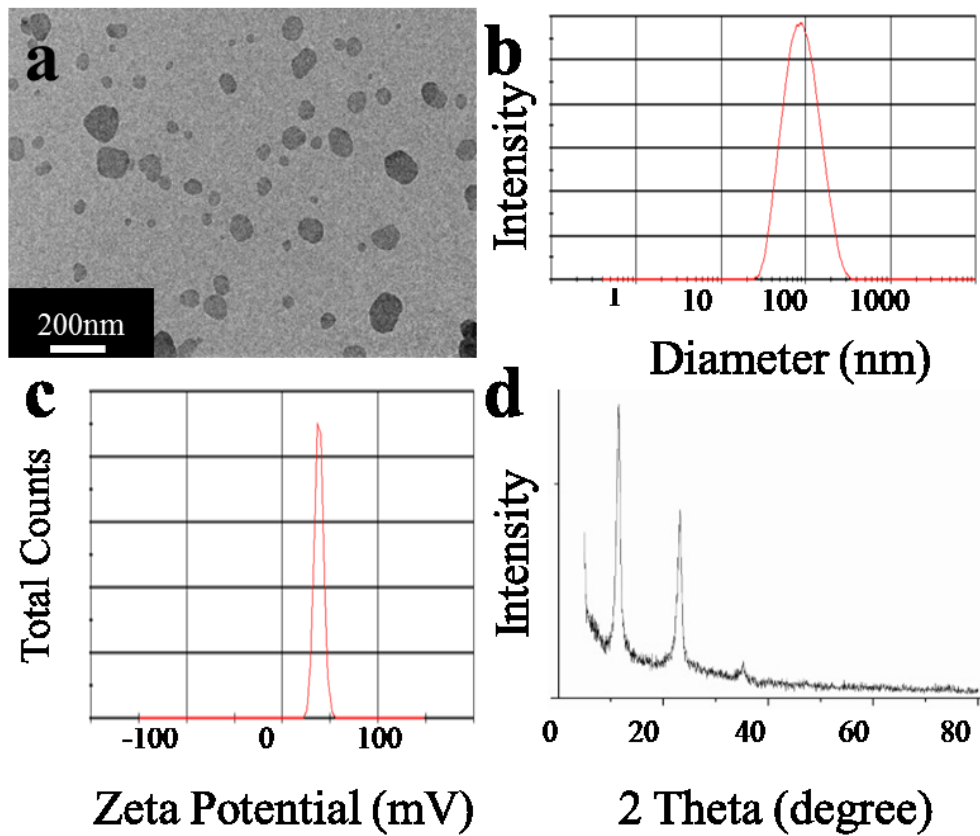
434 *ELISA protocol:* ELISA was performed as previously described.<sup>[36]</sup> Briefly, ELISA plates  
 435 (Corning) were coated with 50 µg mL<sup>-1</sup> of ovalbumin (Acros) in 0.1M of sodium bicarbonate  
 436 buffer (Sigma) overnight at 4°C. These coated plates were used to measure the titers of  
 437 specific IgG induced. Color development was carried out using ABTS (diammonium 2,2-  
 438 azino-bis(3-ethylbenzothiazoline-6-sulfonate; Sigma) as the substrate. The absorbance  
 439 readings at 405 nm were then measured against control wells containing no antiserum in the  
 440 reaction.

441 **Acknowledgements**

442 This study was funded by City University of Hong Kong (Project No. 7200247 and  
443 9667053). We thank Prof. Andrey L Rogach, Dr. Andrei Susha and Dr. Steve Kershaw for  
444 providing research support and useful advices. We also acknowledge Mr TF Hung and Tsz  
445 Chun Lau for SEM observation.

- 446 [1] S. P. Sullivan, D. G. Koutsonanos, M. Del Pilar Martin, J. W. Lee, V. Zarnitsyn, S. O.  
447 Choi, N. Murthy, R. W. Compans, I. Skountzou, M. R. Prausnitz, *Nat. Med.* **2010**, *16*,  
448 915.
- 449 [2] T. W. Prow, X. Chen, N. A. Prow, G. J. P. Fernando, C. S. E. Tan, A. P. Raphael, D.  
450 Chang, M. P. Ruutu, D. W. K. Jenkins, A. Pyke, M. L. Crichton, K. Raphaelli, L. Y. H.  
451 Goh, I. H. Frazer, M. S. Roberts, J. Gardner, A. A. Khromykh, A. Suhrbier, R. A. Hall, M.  
452 A. F. Kendall, *Small* **2010**, *6*, 1776.
- 453 [3] Q. Zhu, V. G. Zarnitsyn, L. Ye, Z. Wen, Y. Gao, L. Pan, I. Skountzou, H. S. Gill, M. R.  
454 Prausnitz, C. Yang, R. W. Compans, *Proc. Natl. Acad. Sci. U. S. A.* **2009**, *106*, 7968.
- 455 [4] S. Liu, M. Jin, Y. Quan, F. Kamiyama, H. Katsumi, T. Sakane, A. Yamamoto, *J. Control.*  
456 *Release* **2012**, *161*, 933.
- 457 [5] X. Chen, H. J. Corbett, S. R. Yukiko, A. P. Raphael, E. J. Fairmaid, T. W. Prow, L. E.  
458 Brown, G. J. P. Fernando, M. A. F. Kendall, *Adv. Funct. Mater.* **2011**, *21*, 464.
- 459 [6] S. Kaushik, A. H. Hord, D. D. Denson, D. V. McAllister, S. Smitra, M. G. Allen, M. R.  
460 Prausnitz, *Anesth. Analg.* **2001**, *92*, 502.
- 461 [7] A. P. Raphael, T. W. Prow, M. L. Crichton, X. Chen, G. J. P. Fernando, M. A. F. Kendall,  
462 *Small* **2010**, *6*, 1785.
- 463 [8] S. P. Sullivan, N. Murthy, M. R. Prausnitz, *Adv. Mater.* **2008**, *20*, 933.
- 464 [9] M.R. Prausnitz, R. Langer, *Nat. Biotechnol.* **2008**, *26*, 1261.
- 465 [10] K. Van der Maaden, W. Jiskoot, J. Bouwstra, *J. Control. Release* **2012**, *161*, 645.
- 466 [11] C. J. Ke, Y. J. Lin, Y. C. Hu, W. L. Chiang, K. J. Chen, W. C. Yang, H. L. Liu, C. C. Fu,  
467 H. W. Sung, *Biomaterials* **2012**, *33*, 5156.
- 468 [12] J. W. Lee, J. Park, M. R. Prausnitz, *Biomaterials* **2008**, *29*, 2113.
- 469 [13] X. Chen, G. J. P. Fernando, M. L. Crichton, C. Flaim, S. R. Yukiko, E. J. Fairmaid, H. J.  
470 Corbett, C. A. Primiero, A. B. Ansaldo, I. H. Frazer, L. E. Brown, M. A. F. Kendall, *J.*  
471 *Control. Release* **2011**, *152*, 349.
- 472 [14] G. J. P. Fernando, X. Chen, T. W. Prow, M. L. Crichton, E. J. Fairmaid, M. S. Roberts, I.  
473 H. Frazer, L. E. Brown, M. A. F. Kendall, *PLoS ONE.* **2010**, *5*, e10266.
- 474 [15] Q. Wang, D. O'Hare, *Chem. Rev.* **2012**, *112*, 4124.
- 475 [16] H. Peng, W. C. Tjiu, L. Shen, S. Huang, C. He, T. Liu, *Compos. Sci. Technol.* **2009**, *69*,  
476 991.
- 477 [17] K. Ladewig, M. Niebert, Z.P. Xu, P.P. Gray, G.Q.M Lu, *Biomaterials* **2010**, *31*, 1821.
- 478 [18] X. Chen, T. W. Prow, M. L. Crichton, D. W. K. Jenkins, M. S. Roberts, I. H. Frazer, G. J.  
479 P. Fernando, M. A. F. Kendall, , *J. Control. Release* **2009**, *139*, 212.
- 480 [19] P. C. DeMuth, W. F. Garcia-Beltran, M. L. Ai-Ling, P. T. Hammond, D. J. Irvine, *Adv.*  
481 *Funct. Mater.* **2013**, *23*, 161.
- 482 [20] P. C. DeMuth, Y. Min, B. Huang, J. A. Kramer, A. D. Miller, D. H. Barouch, P. T.  
483 Hammond, D. J. Irvine, *Nat. Mater.* **2013**, *12*, 367.

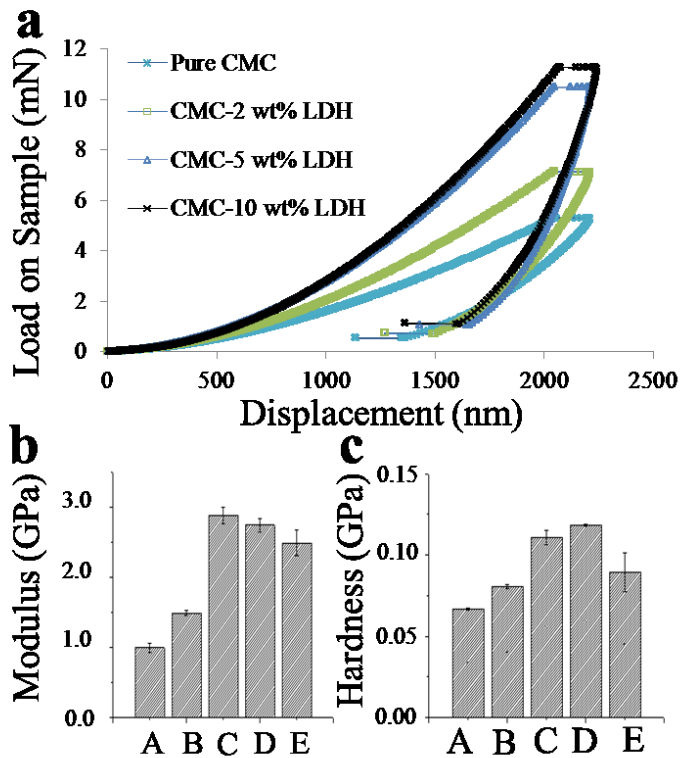
- 484 [21] G. J. P. Fernando, X. Chen, C. A. Primiero, S. R. Yukiko, E. J. Fairmaid, H. J. Corbett, I.  
485 H. Frazer, L. E. Brown, M. A. F. Kendall, *J. Control. Release* **2012**, *159*, 215.
- 486 [22] X. Chen, A. S. Kask, M. L. Crichton, C. McNeilly, S. Yukiko, L. Dong, J. O. Marshak, C.  
487 Jarrahan, G. J. P. Fernando, D. Chen, D. M. Koelle, M. A. F. Kendall, *J. Control.*  
488 *Release* **2010**, *148*, 327.
- 489 [23] N. Falstiejensen, E. Spaun, J. Brochnermortensen, S. Falstiejensen, *Scand. J. Clin. Lab.*  
490 *Invest.* **1988**, *48*, 519.
- 491 [24] J. Choy, J. Jung, J. Oh, M. Park, J. Jeong, Y. Kang, O. Han, *Biomaterials*. **2004**, *25*,  
492 3059.
- 493 [25] J. Oh, S. Choi, G. Lee, S. Han, J. Choy, *Adv. Funct. Mater.* **2009**, *19*, 1617.
- 494 [26] Z. Gu, B. E. Rolfe, A. C. Thomas, J. H. Campbell, G. Q. Lu, Z. P. Xu, *Biomaterials*.  
495 **2011**, *32*, 7234.
- 496 [27] Y. Wong, K. Markham, Z. P. Xu, M. Chen, G. Q. (Max) Lu, P. F. Bartlett, H. M.  
497 Cooper, *Biomaterials*. **2010**, *31*, 8770.
- 498 [28] K. Ladewig, M. Niebert, Z. P. Xu, P. P. Gray, G. Q. M. Lu, *Biomaterials*. **2010**, *31*, 1821.
- 499 [29] Y. Wong, H. M. Cooper, K. Zhang, M. Chen, P. Bartlett, Z. P. Xu, *J. Colloid Interface*  
500 *Sci.* **2012**, *369*, 453.
- 501 [30] L. Desigaux, M. Ben Belkacem, P. Richard, J. Cellier, P. Leone, L. Cario, F. Leroux, C.  
502 Taviot-Gueho, B. Pitard, *Nano Lett.* **2006**, *6*, 199.
- 503 [31] J. Choy, S. Kwak, Y. Jeong, J. Park, *Angew. Chem. Int. Ed.* **2000**, *39*, 4042.
- 504 [32] Z. P. Xu, G. Stevenson, C. Lu, G. Q. Lu, *J. Phys. Chem. B* **2006**, *110*, 16923.
- 505 [33] Z. Xu, G. Stevenson, C. Lu, G. Lu, P. Bartlett, P. Gray, *J. Am. Chem. Soc.* **2006**, *128*, 36.
- 506 [34] R. Bhandari, S. Negi, F. Solzbacher, *Biomed. Microdevices* **2010**, *12*, 797.
- 507 [35] E. M. T. Wurm, C. Longo, C. Curchin, H. P. Soyer, T. W. Prow, G. Pellacani, *Br. J.*  
508 *Dermatol.* **2012**, *167*, 270.
- 509 [36] G. J. P. Fernando, T. J. Stewart, R. W. Tindle, I. H. Frazer, *J. Immunol.* **1998**, *161*, 2421.
- 510 Received: ((will be filled in by the editorial staff))  
511 Revised: ((will be filled in by the editorial staff))  
512 Published online on ((will be filled in by the editorial staff))  
513  
514  
515



516

517 **Figure 1.** a) HRTEM image of well dispersed Mg<sub>2</sub>Al-Cl-LDH nanoparticles. b) Particle size  
518 distribution of Mg<sub>2</sub>Al-LDH suspension. c) The zeta potential of the Mg<sub>2</sub>Al-LDH nanoparticles in  
519 aqueous and buffer-free solution. d) X-ray diffraction pattern of pristine LDH nanoparticles.

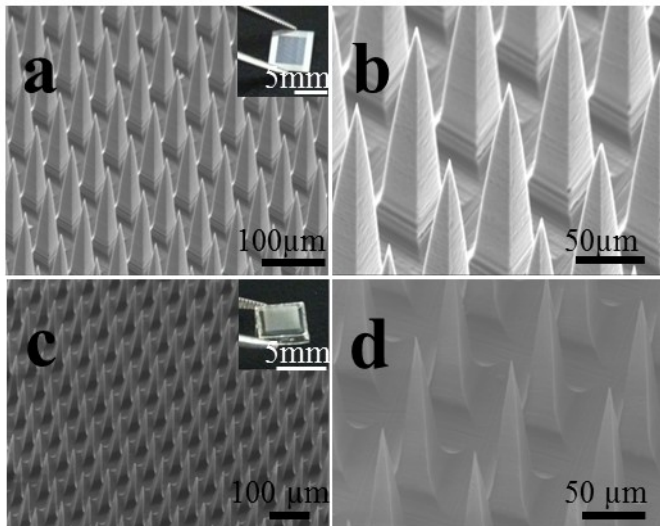
520



521

522 **Figure 2.** a) Load-displacement curves from nanoindentation. b) Elastic modulus and c)  
523 Hardness of CMC polymer films with different LDH concentrations: A-0 wt%; B-2 wt%; C-5  
524 wt%; D-10 wt% and E-5 wt% with centrifugation.

525

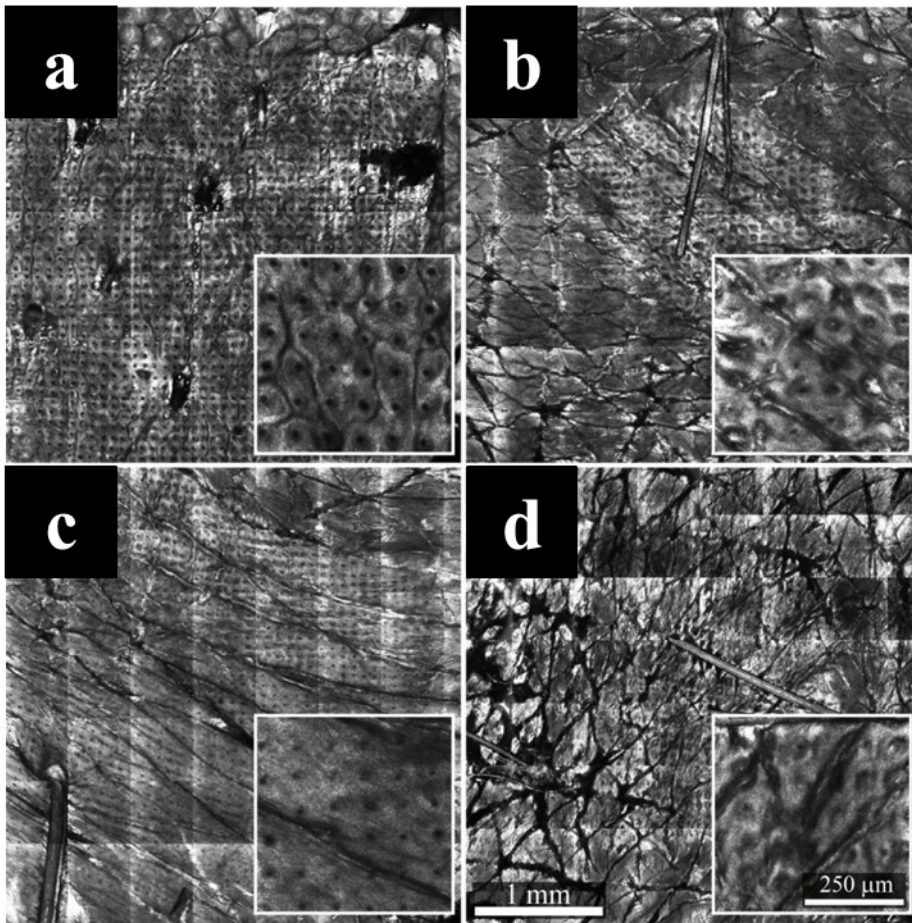


526

527 **Figure 3.** Scanning electron microscopy images of microneedles: a-b) Silicon microneedles  
528 array male mold (inset: digital camera image of a silicon microneedle array); c-d) Fabricated  
529 dissolving polymer microneedles (inset: digital camera image of a polymer microneedle  
530 array).

531

532



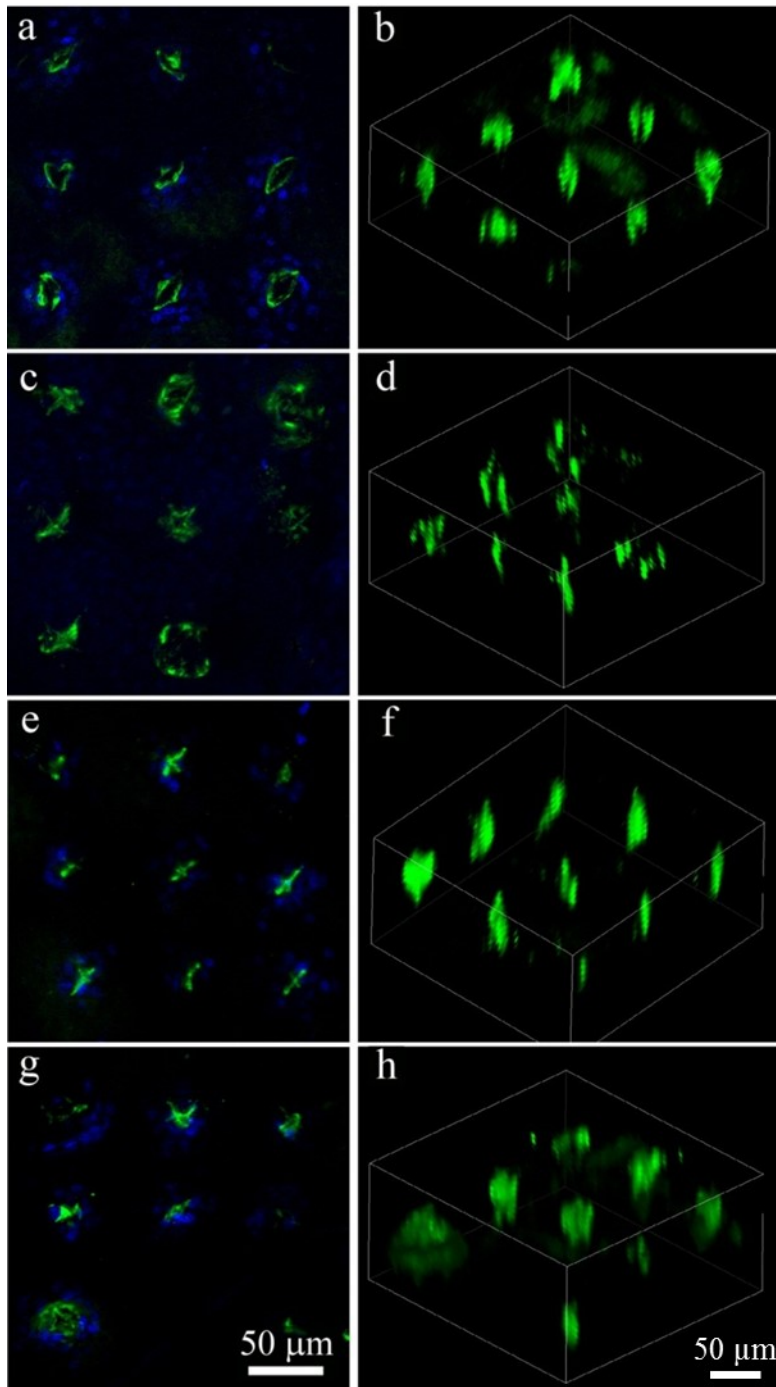
533

534

535 **Figure 4.** Reflectance confocal microscopy images of skin after 5 minutes microneedle  
536 application: a) pig skin after CMC-LDH nanocomposite microneedle application, b) pig skin  
537 after CMC microneedle application, c) human skin after CMC-LDH nanocomposite  
538 microneedle application, and d) human skin after CMC microneedle application.

539

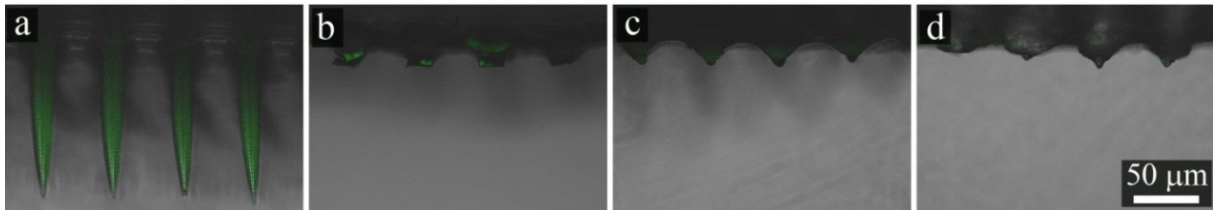
540



541  
542  
543  
544  
545  
546  
547  
548  
549

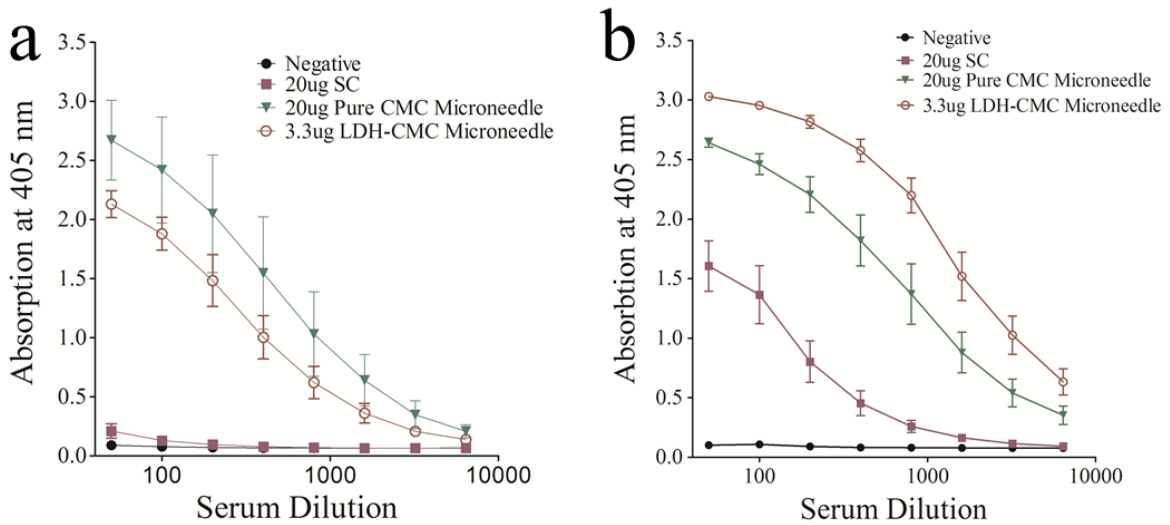
**Figure 5.** Laser scanning confocal microscopy images of skin after 5 minutes microneedle application: a) and b) pig skin after CMC-LDH nanocomposite microneedle application, c) and d) pig skin after CMC microneedle application, e) and f) human skin after CMC-LDH nanocomposite microneedle application, and g) and h) human skin after CMC microneedle application.





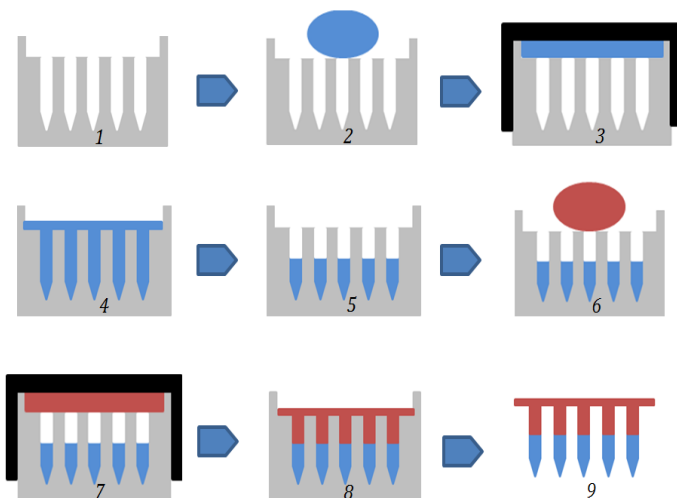
550  
551  
552  
553  
554

**Figure 6.** Merged fluorescence and reflectance confocal microscopy images of CMC-LDH nanocomposite microneedles: a) before application, b) 1 minute, c) 2 minutes and d) 5 minutes after application to pig skin.



555  
556  
557  
558  
559  
560  
561  
562  
563  
564

**Figure 7.** Total ovalbumin IgG levels at 12 and 38 days post vaccination. Five mice were subcutaneously injected with 20  $\mu$ g of OVA protein to be the positive control. Four unimmunized mice were negative control. For microneedle immunization, either pure CMC or CMC-LDH nanocomposite microneedle patches containing different amounts of OVA protein were used to vaccinate the mice. Each group has four mice. Mice were immunized at day 0 and boosted at day 17. At day 14 and 38, sera were collected and assayed for antibody titer measurements. The antibody titers at different dilutions of each group of mice were shown in the figure.



565  
566

**Figure 8.** Steps to manufacture a dissolving nanocomposite microneedle patch.

567 **Highly uniform nanocomposite microneedles array** is fabricated under mild conditions.  
568 These very small and densely packed nanocomposite microneedles can mechanically robust  
569 enough to pierce pig/human skin, rapidly dissolve to release payload in targeted layers and  
570 induce robust immune responses.

571

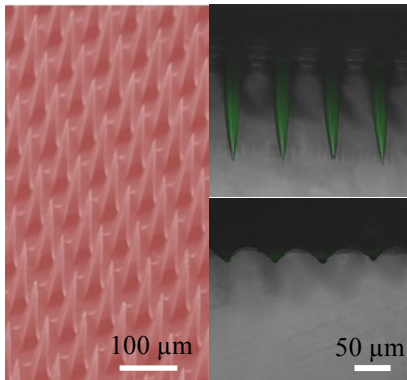
572 Keywords: Transdermal delivery; vaccine delivery; nanocomposite; polymeric material;  
573 biomedical applications

574

575 Li Yan, Anthony P Raphael, Xiaoyue Zhu, Beilei Wang, Wei Chen, Tao Tang, Yan Deng,  
576 Himanshu J Sant, Guangyu Zhu, Kwong Wai Choy, Bruce K Gale, Tarl W Prow, and  
577 Xianfeng Chen\*

578

579 **Nanocomposite strengthened dissolving microneedles for improved transdermal**  
580 **delivery to human skin**



581

582

583

584 Page Headings

585 Left page: First Author et al.

586 Right page: Title of manuscript (abbreviated)